DOI:10.1478/C1A0501002

Atti dell'Accademia Peloritana dei Pericolanti
Classe di Scienze Fisiche, Matematiche e Naturali
Vol. LXXXIII, C1A0501002 (2005-06)
Adunanza del 16 maggio 2005

MICROSCOPIC THEORY OF SPATIALLY RESOLVED PHOTOLUMINESCENCE IN DISORDERED NANOSTRUCTURES

S. SAVASTA, G. MARTINO,* G. PISTONE, O. DI STEFANO, and R. GIRLANDA

(Nota presentata dal Socio Ordinario Raffaello Girlanda)

ABSTRACT. Quantum dots have become objects of extensive research activity because of their applications such as advanced electronic and optoelectronic devices. Here we analyse theoretically the optical properties of dots naturally formed by interface fluctuations in GaAs narrow quantum wells. Specifically we present the simulations of local optical spectroscopy and spatially resolved photoluminescence in quantum wells with interface fluctuations. The theory includes light quantization, acoustic phonon scattering, and inhomogeneous sample-excitation and/or light-detection. Such theoretical framework provides a general basis for the description of spectroscopic imaging. Numerically calculated absorption and photoluminescence images clarify the impact of the near-field optical setup and put forward the potentials of the method for the understanding of near-field light emission from semiconductor quantum structures.

1. Introduction

The introduction of improved semiconductor growth techniques over the past few decades have allowed physical realisation of nanostructured systems. Semiconductor nanostructures exhibit interesting new behavior and would be highly desirable for future applications, for example in the area of quantum information processing, for various technological applications such as enhanced optoelectronic devices, single photon emitters and detectors based on quantum dot (QD) systems.

Really the definition of the interfaces on an atomic scale is never as ideal as physicists would like it to be. Even with the most sophisticated growth techniques, interface fluctuations of one or a few monolayers can hardly be avoided. A further source of disorder is alloy fluctuation if a ternary compound is used as barrier or well material. So these disorder effects determine the inhomogeneous broadening of the exciton line seen in optical measurements, and even tend to dominate their linewidth in narrow quantum structures and to localize the center of mass (COM) motion of excitons [1].

In this context, the availability of characterizing tools is of primary importance. Macroscopic optical probes [2, 3] as photoluminescence (PL), photoluminescence excitation spectroscopy (PLE), and ultrafast Rayleigh scattering have proven to be powerful techniques for probing localized excitons and hence interface fluctuations of quantum structures. However, such probes perform a spatial averaging of the spectral signal, providing information at best on an inhomogeneous ensemble of almost zero-dimensional localized

states of the COM motion. Near-field optical microscopy and spectroscopy, which uses optical interaction in the visible or near-infrared range has recently become a irreplaceable technique for optical imaging and spectroscopy at sub-diffraction resolution. Confining the optical excitation to a very small volume below the diffraction limit, implies the presence of optical fields with high lateral spatial frequencies able to excite surface states with high k vectors not accessible by far-field optical excitations. As a consequence optical spectra of homogeneous surface systems can display remarkable differences in the near and far zones [4, 5].

This kind of optical microscopy and spectroscopy is able to identify the individual quantum constituents of semiconductor quantum structures [3, 6, 7, 8], can bring to direct and complete quantum mechanical information on the spatial variations of solid-state mesoscopic quantum eigenfunctions [9] and provides new insights into the nonlocal character of light-matter interaction [10, 11]. The high spatial resolution is obtained in Scanning Near field Optical Microscopy (SNOM) experiments by means of a tapered optical probe used to obtain the desired spatially confined excitation and/or light-detection.

Theoretical simulations of near-field imaging spectroscopy of semiconductor quantum structures generally focus on calculation of local absorption [11, 12, 13, 14], while almost all experimental images are obtained from PL measurements. The supposed equivalence between PLE and absorption spectra in semiconductors structures is based on the assumption that the recombination times are much larger than the intraband ralaxation times [15]. In this situation, the emission intensity is nearly independent of the relaxation rate and the luminescence spectrum does not coincide with the absorption spectrum.

Detailed simulations of Zimmermann et al. have clarified many aspects of the intrigued non-equilibrium dynamics giving rise to photoluminescence spectra in disordered quantum structures [16, 17]. Since direct observation of zero dimensional (0D) semiconductor QDs naturally occurred in narrow quantum wells by near-field photoluminescence imaging they have attracted great attention [3, 18]. Here we present a microscopic quantum theory of spatially and spectrally resolved photoluminescence in quantum structures that includes both light quantization (essential to describe spontaneous emission) and phonon scattering. The theory includes the description of spatially confined excitation (illumination mode) and/or detection (collection mode). Thus this formulation permits one to model spectroscopic imaging based on PL excitation spectroscopy in which the excitation and detection energies and spatial positions can all independently be scanned.

In particular we simulate the construction of reasonable good quality GaAs QW in between $Al_xGa_{1-x}As$ barrier (see Fig. 1). In this case, we can suppose that the motion of an electron-hole pair happens in a disorder potential that acts only on the center of mass coordinate. This is a good assumption only if the amplitude of the disorder potential does not exceed the exciton binding energy. We report spectroscopic images obtained in collection mode configuration, where the sample is illuminated conventionally and aperture-SNOM (tip) is used to collect locally the scattered light.

2. Theory

The positive frequency components of the operator describing the signal that can be detected by a general near-field setup can be expressed as [19]

$$\hat{S}_t^+ = \hat{A}_{bg}^+ + \hat{S}^+ , \tag{1}$$

where $\hat{A}_{bg}^+$ is the elastic background signal, largely uniform along the $x-y$ plane; this term is proportional to the input electric-field operator. $\hat{S}^+$ is related to the sample polarization density operator $\hat{\mathbf{P}}^+(\mathbf{r})$,

$$\hat{S}^+ = \mathcal{A} \int d\mathbf{r}\, \hat{\mathbf{P}}^+(\mathbf{r}) \cdot \mathbf{E}_{out}(\mathbf{r}) , \tag{2}$$

where $\mathcal{A}$ is a complex constant depending on the impedance of the material constituting the tip [19] and $\mathbf{E}_{out}(\mathbf{r})$ is the field mode delivered by the tip. The interband polarization density operator is given by

$$\hat{\mathbf{P}}^+(\mathbf{r}) = \sum_{eh} \boldsymbol{\mu}_{eh}\, \hat{c}_e(\mathbf{r}) \hat{d}_e(\mathbf{r}) . \tag{3}$$

Here, e and h are appropriate sets of quantum numbers which label the carrier states involved in the optical transition. Photoluminescence can be defined as the incoherent part of the emitted light intensity. The PL that can be measured by a photodetector after the collection setup (broadband detection) is proportional to $I = \langle\, \hat{S}^- , \hat{S}^+ \,\rangle$, (with $\langle\, \hat{A} , \hat{B} \,\rangle \equiv \langle\, \hat{A}\, \hat{B} \,\rangle - \langle\, \hat{A} \,\rangle \langle\, \hat{B} \,\rangle$). Analogously the steady-state spectrum of incoherent light emitted by the semiconductor quantum structure and detected by the SNOM setup can be expressed as

$$I_{PL}(\omega_{out}) = \frac{1}{\pi} \int_0^\infty d\tau\, \langle\, \hat{S}^-(0) , \hat{S}^+(\tau) \,\rangle\, e^{i\omega_d \tau} . \tag{4}$$

The polarization density operator can be expressed in terms of exciton operators as,

$$\hat{\mathbf{P}}^+(\mathbf{r}) = \boldsymbol{\mu}_{eh} \sum_\alpha f(z) \Psi_\alpha^{eh}(\rho = 0, \mathbf{R}) \hat{B}_\alpha . \tag{5}$$

The operator $\hat{B}_\alpha^\dagger$ creates an exciton state (one electron-hole pair) $\hat{B}_\alpha^\dagger |0\rangle \equiv |E_{1,\alpha}\rangle$ with energy $\omega_{1,\alpha}$. $\Psi_\alpha^{eh}(\rho, \mathbf{R})$ is the exciton wavefunction with ρ indicating the relative in-plane eh coordinate and $\mathbf{R}$ describes the centre of mass motion, while $f(z) = u_e(z) u_h(z)$ is the product of the electron and hole envelope functions along the confinement direction (the growth axis). If the disorder induced broadening is small compared to the exciton binding energy, only the lowest bound state 1s at the fundamental sublevel transition has to be considered and the exciton wave function can be factorized as follows [17]

$$\Psi_\alpha^{eh}(\rho, \mathbf{R}) = \phi_{1s}(\rho) \psi_\alpha(\mathbf{R}). \tag{6}$$

where

$$\psi_\alpha(\mathbf{R}) \tag{7}$$

are solutions of the following center mass equation

$$\left(-\frac{\hbar^2\nabla^2}{2M}+V(\mathbf{R})\right)\psi_\alpha(\mathbf{R})=\epsilon_\alpha\psi_\alpha(\mathbf{R}) \tag{8}$$

where V(R) is the effective random potential resulting from well-width fluctuations, and $M = m_e^* + m_h^*$ is the exciton kinetic mass (m_e^* and m_h^* are the effective masses of the electron and the hole).

The dynamics controlled truncation scheme [20] provides an upper limit to the number of electron-hole pairs to be included for the dynamics description of the interacting electron system, depending on the excitation density. States with only one electron-hole pair (excitons) are sufficient to describe the system dynamics at low excitation densities. In this regime the following relation can be assumed,

$$\hat{B}_\alpha \simeq |0\rangle \langle E_{1,\alpha}| \ , \tag{9}$$

and it can be shown that the operators $\hat{B}_\alpha$ behave as Boson operators. Including only the exciton subspace and using Eq. (9), the Hamiltonian determining the dynamics of the semiconductor system is given by the following three contributions:

$$H = H_0 + H_I + H_s, \tag{10}$$

where the first term is the bare electronic Hamiltonian of the semiconductor system $H_0 = \sum_\alpha \hbar\omega_\alpha \hat{B}_\alpha^\dagger \hat{B}_\alpha$. The interaction of the semiconductor with the light field (in the usual rotating wave approximation) can be written as

$$H_I = -\int d^3r\, \hat{\mathbf{E}}^-(\mathbf{r})\cdot\hat{\mathbf{P}}^+(\mathbf{r}) + H.c.\,. \tag{11}$$

We separate the field operator into a classical contribution $\mathbf{E}_{in}(\mathbf{r})$ describing the (possible inhomogeneous) exciting field and into a fluctuating part $\hat{\mathcal{E}}^-(\mathbf{r})$ (the one determining the spontaneous emission) that can be expanded in terms of annihilation photon operators. Finally H_s describes inelastic scattering due to the interaction of excitons with the phonon bath.

$$H_s = \sum_{\alpha,\beta,\mathbf{q}} t^{\mathbf{q}}_{\alpha,\beta}(b_{\mathbf{q}} + b^\dagger_{-\mathbf{q}})\hat{B}^\dagger_\alpha \hat{B}_\beta \,, \tag{12}$$

These terms produce scattering between different exciton states and dephasing. For the lowest exciton states, scattering with acoustic phonons is in most cases the dominant process. $b_{\mathbf{q}}$ is the Bose annihilation operator for a phonon with wave vector $\mathbf{q}$. The scattering matrix elements depend on the lattice deformation potentials and the overlap between the exciton states. The explicit expression for $t^{\mathbf{q}}_{\alpha,\beta}$ can be found elsewhere [17].

The relaxation process in the low-excitation limit can be discussed in terms of kinetic equation for the exciton density matrix. Diagonal terms of the exciton density matrix $N_\alpha = \left\langle \hat{B}^\dagger_\alpha \hat{B}_\alpha \right\rangle$, can be derived starting from the Heisenberg equation of motion for the exciton operators

$$-i\hbar\partial_t \hat{B}^\dagger_\alpha(t) = \left[\hat{\mathcal{H}}, \hat{B}^\dagger_\alpha(t)\right] \tag{13}$$

under the influence of H.

The main approximations are the neglect of possible coherent phonon states and of

memory effects induced by the photon and phonon fields. The kinetic equation that consider a spatially resolved (illumination-mode) input light field of given frequency ω_{in} and allows to study the temperature dependence is

$$\partial_t N_\alpha = G_\alpha(\omega_{in}) + \sum_\beta \gamma_{\alpha\leftarrow\beta} N_\beta - 2\Gamma_\alpha N_\alpha \,, \tag{14}$$

where $2\Gamma_\alpha = r_\alpha + \sum_\beta \gamma_{\beta\leftarrow\alpha}$ is the total out-scattering rate, r_α is the rate for spontaneous emission proportional to the exciton oscillator strength: $r_\alpha = r_0 \left| \int d^2\mathbf{R}\, \psi_\alpha(\mathbf{R}) \right|^2$, and $\gamma_{\beta\leftarrow\alpha}$ are the resulting phonon-assisted scattering rates [17], given by

$$\gamma_{\beta\leftarrow\alpha} = \frac{2\pi}{\hbar} \sum_{\mathbf{q}} \left((n_{\mathbf{q}}+1)\,\delta(\epsilon_\beta + \hbar\omega_{\mathbf{q}} - \epsilon_\alpha) + n_{\mathbf{q}}\delta(\epsilon_\beta - \hbar\omega_{\mathbf{q}} - \epsilon_\alpha) \right) \left| t^{\mathbf{q}}_{\beta\alpha} \right|^2 . \tag{15}$$

An explicit calculation of r_0 can be found elsewhere (see appendix C of ref. [17]).

Here we assume that the tip-sample interaction does not alter the radiative decay rates. In this equation the generation term that describes the specific experimental excitation conditions, depends on the spatial overlap between the illuminating beam and the exciton wavefunctions corresponding to exciton levels resonant with the input light [21]:

$$G_\alpha = r_0 \left| o^{in}_\alpha \right|^2 \mathcal{L}_\alpha(\omega_{in}) \tag{16}$$

with $\pi\mathcal{L}_\alpha(\omega) = \Gamma/[(\omega-\omega_\alpha)^2 + \Gamma^2]$ and

$$o^{in}_\alpha = \int d^2\mathbf{R}\, \tilde{E}_{in}(\mathbf{R}) \psi_\alpha(\mathbf{R}) \tag{17}$$

where $\tilde{E}_{in}(\mathbf{R}) = \int E_{in}(\mathbf{r}) f(z) dz$.

In the subsequent numerical calculations concerning the illumination-mode we will assume an input light field with a given Gaussian profile centered around the tip position: $\tilde{E}_{in}(\mathbf{R}) = E^0_{in} g(\mathbf{R} - \bar{\mathbf{R}})$. In this case the generation term becomes function of the beam position and shape (spatial resolution). We observe that also at steady-state Eq. (14) can give rise to highly non-equilibrium exciton densities. Non-equilibrium here arises from both spontaneous emission that prevents full thermalization and from the eventual local excitation described by the generation terms.

Once the exciton densities have been derived, the frequency integrated PL can be readily obtained. Inserting Eq. (5) into Eq. 2, it results

$$I = r_0 \sum_\alpha \left| o^{out}_\alpha \right|^2 N_\alpha \,, \tag{18}$$

where o^{out}_α analogously to o^{in}_α contains the overlap of the exciton wavefunctions with the signal mode $\tilde{E}_{out}(\mathbf{R})$ delivered by the tip (collection mode) and is given by

$$o^{out}_\alpha = \int d^2\mathbf{R}\, \tilde{E}_{out}(\mathbf{R}) \psi_\alpha(\mathbf{R}) \tag{19}$$

According to the quantum regression theorem, $\left\langle \hat{S}^-(0)\, \hat{S}^+(\tau) \right\rangle$ has the same dynamics of $\left\langle \hat{S}^+(\tau) \right\rangle$ (proportional to the exciton operator), but with $\left\langle \hat{S}^-(0)\, \hat{S}^+(0) \right\rangle$ as initial

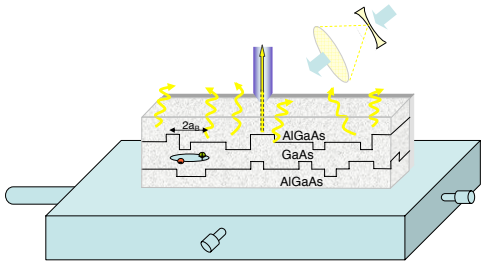

FIGURE 1. Schematic view of the exciton in a ternary QW with rough interfaces

condition. Following this procedure we obtain

$$I_{PL}(\omega_{out}) = r_0 \sum_{\alpha} \left| o_{\alpha}^{out} \right|^2 \mathcal{L}_{\alpha}(\omega_{out})\, N_{\alpha} \tag{20}$$

3. Numerical results

Here we present numerical result of spatially and spectrally resolved PL for a system of QDs arising from interface fluctuations of GaAs quantum wells.

We consider the system Hamiltonian containing the disordered potential described afterwards. Eigenvalues and eigenvectors are obtained using the relevant LAPACK library routines available online at [22]. Then we calculate the overlaps between the exciton states, the source terms and the scattering rates, so to finally write the kinetic equation for the exciton occupation (14). The system of linear equations deriving from putting this equation equal to zero (stationary case) is solved using the LAPACK routines again; the resulting N_α are inserted in Eqs. (18) and (20) in order to obtain the desired PL intensities. The effective disordered potential $V(\mathbf{r})$, used in our simulations is obtained summing up two different contributions. They are both modelled as a zero mean, Gauss distributed and spatially correlated process defined by the property $\langle\ V(\mathbf{r})V(\mathbf{r}')\ \rangle = v_0^2 e^{-\left|\mathbf{r}-\mathbf{r}'\right|^2/2\xi^2}$, where $\langle\ \ldots\ \rangle$ denotes ensemble average over random configurations, v_0 is the width of the energy distribution, and ξ is the correlation length characterizing the potential fluctuations. For the former potential we have chosen $\xi = 16$ nm and $v_0 = 1.5$ meV; for the latter, we used $\xi = 8$ nm and $v_0 = 0.5$ meV. Fig. 2(a) shows the effective disordered potential felt by excitons obtained summing these two contributions and used for all the calculations. The white circle specify the location chosen for local detection.

The samples so characterized take into account two different types of disorder occurring in the real structures: one encountered in studies of islandlike defects in II-VI quantum well [3] (where the lateral extent of the confining potential is comparable to or much largher than the exciton diameter) or self-assembled III-V QDs [23] (where 0D confinement occurs in islands with a larger height-diameter ratio) and the other considered by Flack [24], where the samples are characterized by potential fluctuations at length scales small compared to the exciton diameter.

As a prototype we consider GaAs QWs sandwiched by $Al_xGa_{1-x}As$ barriers, and adopt an exciton kinetic mass of $m = 0.25m_0$. By considering a square region of 540

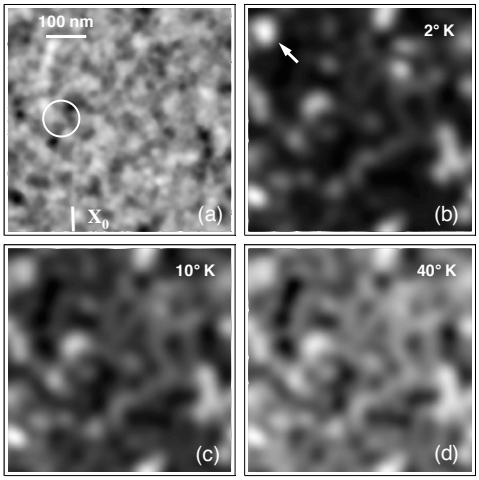

FIGURE 2. (a) Specific realization of disorder potential (parameters are given in the text). (b-d) Energy-integrated PL images obtained after uniform illumination of the sample at energy $\omega_I = 1$ meV and collecting locally the emitted light.

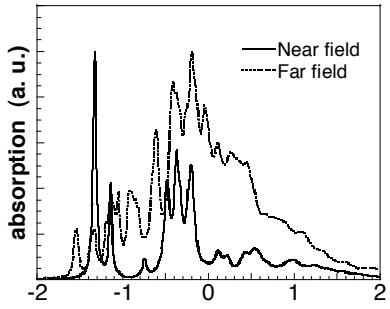

FIGURE 3. Far field spectrum and local absorption spectrum calculated centering the tip at the position indicated by the circle in Fig. 2 (a)

nm by 540 nm, we obtain a three dimensional matrix of data $I(x, y, \omega)$ where x and y are position coordinates.

In Fig. 2(b-d) we present energy-integrated PL images obtained after uniform illumination of the sample at energy $\omega_I = 1$ meV (the zero of energy is fixed at the energy of the 1s exciton in absence of disorder) and collecting locally the emitted light (C mode with spatial resolution $FWHM = 47$ nm). It is worth noting that the energy integrated excitonic local density of states does not depend on position. So the observed structures are a direct consequence of the increasing ratio between radiative and nonradiative scattering rates for exciton states localized at the potential minima (compare e.g. images a and c). As the

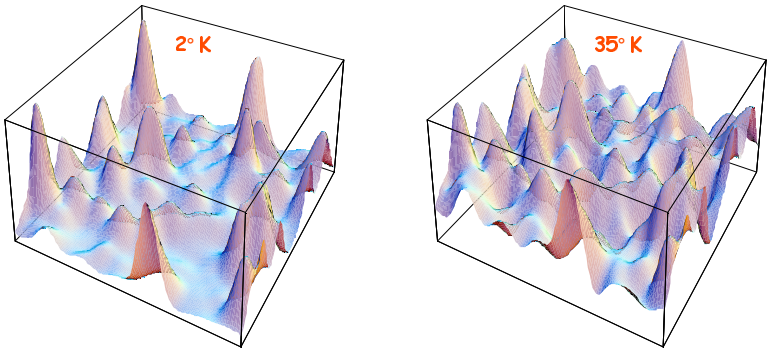

FIGURE 4. Energy integrated spatially resolved photoluminescence at two different temperature

temperature of the structure is lowered, a transition from a broad and fairly continuous PL to an intense set of few spatially localized luminescence centers can be observed. Another interesting feature is the non-monotonous brightness of some luminescence centers when the temperature is increased (see e.g. the location indicated by an arrow in image b), which can be due to a redistribution of excitons that can overcome shallow local minima by thermal activation and fall down in still deeper states. This temperature-dependent behavior is in close analogy with the non-monotonous Stokes shift of PL spectra in dependence of temperature described in many papers [25, 26, 27].

In Fig. 3 we report for reference the far field and a local absorption spectra calculated with the beam position centered in a local minimum of the disordered potential indicated by the circle in Fig. 2(a). The shape of near-field spectrum significantly differs from far field one and strongly depends, as shown elsewhere [14] from the position of the tip. For example, the high-energy contributions are enhanced when the beam position is centered in proximity of a local maximum [14]. Fig. 4 displays two energy-integrated PL images I(X,Y) obtained at two different temperatures (T=2 K and 35 K respectively) It can be instructive to better understand the emission mechanisms of these systems to compare measurements of spatially resolved absorption spectra (recently an indirect method able to provide information on near-field absorption has been developed [28]) with corresponding PL spectra. Near-field optical spectroscopy technique allows us to construct a PL image as a function of the energy by collecting spectra as the tip is rastered over the sample surface.

Fig. 5 displays absorption and the corresponding photoluminescence line-scans spectra calculated at $T = 4^{\circ}\ K$ for the sample. These line-scans are function of the beam position and energy $I_{PL}(X_0, Y, \omega)$ with X_0 fixed (see Fig. 2(a) in order to examine the X_0 direction). We observe how in the PL spectrum (Fig. 5(b)) evidence of states at higher energies due to the continuous band coming from quasi 2D states originating from the potential barriers, present in the absorption spectrum (Fig. 5(a)), disappears. This originates from the fact that for these states energy relaxation due to phonon scattering is much more rapid then the radiative decay rate.

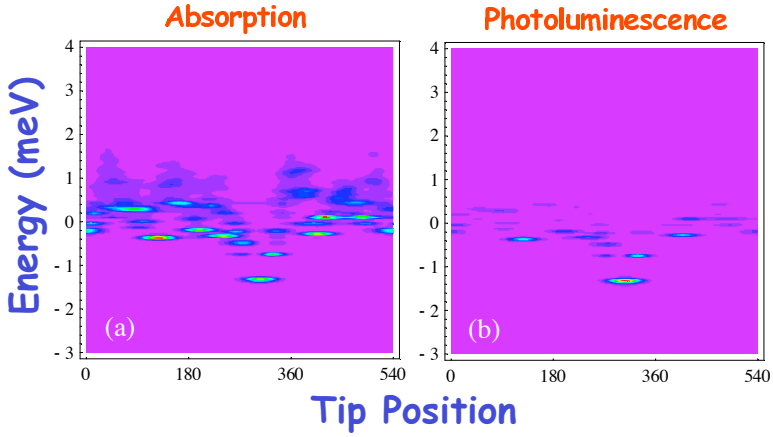

FIGURE 5. Line scan spectra obtained as a function of the beam position and energy $I_{PL}(X_0, Y, \omega)$ with X_0 fixed. (a) Absorption spectrum. (b) Photoluminescence spectrum. The temperature of the sample is $T = 4^{\circ}\ K$. Spatial resolution of the collecting tip: $FWHM = 47$ nm.

4. Conclusion

We have presented a microscopic quantum description of spatially resolved photoluminescence in QWs with interface fluctuations. The theory includes light quantization in order to describe spontaneous emission, acoustic phonon scattering and the description of spatially confined excitation (illumination mode) and/or detection (collection mode). This model is managed to reproduce PL excitation spectroscopy in which the excitation and detection energies and spatial positions can all independently be scanned. The presented numerical calculations show that the assumption of equivalence between PLE and absorption spectra is not justified. In fact, we find significant differences and states at higher energy observed in the PL spectrum, in the absorption spectrum disappears. Moreover, the effect of temperature on the exciton photoluminescence images obtained after uniform illumination of the sample and collecting locally the emitted light has been studied. In particular, we have analyzed how lowering temperature the PL spectra exhibit a metamorphosis from a quantum well system to a quantum dots one. In conclusion we have seen as the numerical results here presented constitute an intriguing example of the impact of sample temperature, exciton localization, and microscope setup in the formation of subwavelength-resolution images.

References

[1] E. Runge and R. Zimmermann, *Phys. Status Solidi B* **206**, 167 (1998).
[2] V. Savona, S. Haake, and B. Deveaud, *Phys. Rev. Lett.* **84**, 183 (2000).
[3] H. F. Hess, E. Betzig, T. D. Harris, L. N. Pfeiffer, and K. W. West, *Science* **264**, 1740 (1994).
[4] S. Savasta, G. Martino, and R. Girlanda, *Phys. Rev. B* **61**, 13852 (2000).
[5] A. V. Shchegrov, K. Joulain, R. Carminati, and J. J. Greffet, *Phys. Rev. Lett.* **85**, 1548 (2000).
[6] D. Gammon, E. S. Snow, and D. S. Katzer, *Appl. Phys. Lett.* **67**, 2391 (1995).
[7] D. Gammon, E. S. Snow, B. V. Shanabrook, D. S. Katzer, and D. Park, *Phys. Rev. Lett.* **76**, 3005 (1996); Science **273**, 87 (1996).

[8] Q. Wu, R. D. Grober, D. Gammon, and D. S. Katzer, *Phys. Rev. Lett.* **83**, 2652 (1999).
[9] O. Di Stefano, S. Savasta, G. Pistone, G. Martino, and R. Girlanda, *Phys. Rev. B* **68**, 165329 (2003).
[10] K. Matsuda, T. Saiki, S. Nomura, M. Mihara and Y. Aoyagi, *Appl. Phys. Lett.* **81**, 2291 (2002).
[11] O. Mauritz, G. Goldoni, F. Rossi, and E. Molinari, *Phys. Rev. Lett.* **82**, 847 (1999).
[12] O. Di Stefano, S. Savasta, G. Martino, and R. Girlanda, *Appl. Phys. Lett.* **77**, 2804 (2000).
[13] O. Di Stefano, S. Savasta, and R. Girlanda, *J. Appl. Phys.* **91**, 2302 (2002).
[14] G. Pistone, S. Savasta, O. Di Stefano, and R. Girlanda, *Phys. Rev. B* **67**, 153305 (2003).
[15] K. Hannewald, S. Glutsch, F. Bechstedt, *Phys. Stat. Sol. (b)* **238**, 517 (2003)
[16] R. Zimmermann and E. Runge, *Phys. Status Solidi (a)* **164**, 511 (1997).
[17] R. Zimmermann, E. Runge, and S. Savona, *Theory of resonant secondary emission: Rayleigh scattering versus luminescence*, in "Quantum Coherence, Correlation and Decoherence in Semiconductor Nanostructures" (Ed. T. Takagahara), Elsevier Science (USA), p. 89-165 (2003).
[18] A. Zrenner, L. V. Butov, M. Hagn, G. Abstreiter, G. Böhm, and G. Weimann, *Phys. Rev. Lett.* **72**, 3382 (1994).
[19] J.-J. Greffet and R. Carminati, *Progress in Surface Science* **56**, 133 (1997).
[20] V. M. Axt, K. Victor, and A. Stahl, *Phys. Rev. B* **53**, 7244 (1996).
[21] G. Pistone, S. Savasta, O. Di Stefano, and R. Girlanda, *Appl. Phys. Lett.* **84**, 2971 (2004).
[22] http://www.netlib.org/lapack.
[23] J. Y. Marzin, J. M. Grard, A. Izral, D. Barrier and G. Bastard, *Phys. Rev. Lett.* **73**, 716 (1994).
[24] F. Flack, N. Samarth, V. Nikitin, P. A. Crowell, J. Shi. Levy and D. D. Awschalom, *Phys. Rev B* **54**, R17312 (1996).
[25] M. S. Skolnick, P. R. tapster, S. J. Bass, A. D. Pitt, N. Apsley, and S. P. Aldred, *Semicon Sci. Technol.* **1**, 29 (1986).
[26] S. T. Davey, E. G. Scott, B. Wakefield, and G. J. Davies, *Semicon Sci. Technol.* **3**, 365 (1988).
[27] E. M. Daly T. J. Glynn, J. D. Lambkin, L. Considine, and S. Walsh, *Phys. Rev. B* **52**, 4696 (1995).
[28] J. R. Guest, T. H. Stievater, Gang Chen, E. A. Tabak, B. G. Orr, D. G. Steel, D. Gammon and D. S. Katzer, *Science* **293**, 2224 (2001).

Salvatore Savasta, Giovanna Martino, Giuseppe Pistone, Omar Di Stefano, Raffaello Girlanda
Università degli Studi di Messina
Dipartimento di Fisica della Materia
e Tecnologie Fisiche Avanzate
Salita Sperone, 31
98166 Messina, Italy
* **E-mail**: giovi@unime.it

Presented: May 16, 2005
Published on line on November 23, 2005